

DOI: 10.1002/adem.201500143

Phase Transformations in Ti–Fe Alloys Induced by High-Pressure Torsion**

By B. B. Straumal,* A. R. Kilmametov, Yu. Ivanisenko, A. S. Gornakova, A. A. Mazilkin, M. J. Kriegel, O. B. Fabrichnaya, B. Baretzky and H. Hahn

The Ti–Fe alloys are quite important among various Ti-based alloys doped with β -stabilisers. Severe plastic deformation by the high pressure torsion (HPT) leads to the strong grain refinement in Ti–Fe alloys. The high-pressure ω Ti-phase appears during HPT of the Ti–1 wt.% Fe alloy. However, the ω Ti does not appear after uniaxial compression at the same pressure, without torsion. ω Ti remains quenched after pressure release and disappears by heating around 140–150 °C. However, the further alloying with iron suppresses the formation of ω Ti-phase. As a result, ω Ti does not appear after HPT in the Ti–10 wt.% Fe alloy.

1. Introduction

The combination of low density (4 500 kg m⁻³), excellent mechanical properties (strength \approx 1 000 MPa, ductility \approx 10%), and good corrosion resistance makes titanium and its alloys one of the best engineering materials.^[1] The structure and properties of titanium alloys can be tailored by using the combination of alloying, as well as thermal and mechanical treatments.^[2,3] They are especially effective because titanium has different allotropic modifications at low (α -phase) and high (β -phase) temperatures. Titanium has also a high-pressure ω -phase. It is supposed that the reversible transformations of α -Ti and β -Ti to the high-pressure phase ($\alpha \leftrightarrow \omega$ and $\beta \leftrightarrow \omega$) can improve the mechanical

properties of the titanium-based alloys. For a targeted thermo-mechanical treatment of the Ti alloys, a detailed knowledge on the fundamentals of the ω -phase formation at high pressure and the phase stability at elevated temperatures is very important. Unfortunately, such data are very scarce up to now.

In Figure 1 the equilibrium “temperature–pressure” phase diagram for pure titanium obtained by in situ experiments under hydrostatic pressure is shown.^[4–13] In pure titanium, the high-pressure phase transition from α -Ti to ω -Ti takes place.^[4–6,8–13] The α – ω – β triple point was experimentally determined at 640 °C and 7.5 GPa.^[10] At room temperature, the $\alpha \rightarrow \omega$ transition occurs between 2.9 and

[*] Prof. B. B. Straumal, Dr. A. S. Gornakova,
Dr. A. A. Mazilkin
Institute of Solid State Physics, Russian Academy
of Sciences, 142432 Chernogolovka,
Russia
Prof. B. B. Straumal, Dr. A. R. Kilmametov,
Dr. Y. Ivanisenko, Dr. A. A. Mazilkin, Dr. B. Baretzky,
Prof. H. Hahn
Karlsruhe Institute of Technology, Institute of
Nanotechnology, 76344 Eggenstein-Leopoldshafen,
Germany
Prof. B. B. Straumal
Moscow Institute of Physics and Technology,
State University, 141700 Dolgoprudny, Russia
Laboratory of Hybrid Nanomaterials, National University of
Science and Technology, 119049 Moscow, Russia
E-mail: straumal@issp.ac.ru

Dr. A. R. Kilmametov
Institute of Physics of Advanced Materials, Ufa
State Aviation Technical University, 450000 Ufa,
Russia
Dr. M. J. Kriegel, Dr. O. B. Fabrichnaya
TU Bergakademie Freiberg, Institut für Werkstoffwissenschaft,
09599 Freiberg, Germany

[**] The work was partially supported by the Deutsche Forschungsgemeinschaft, Russian Foundation for Basic Research grants 12-03-00894, and 16-53-12007), the Ministry of Education and Science of the Russian Federation in the framework of Increase Competitiveness Program of NUST «MISiS» (grant K2-2014-013) and for the grant 14. A12.31.0001, Programme “New Materials” of RAS, and Karlsruhe Nano Micro Facility operated by the by the Karlsruhe Institute of Technology. (Supporting Information is available online from Wiley InterScience or from the author).

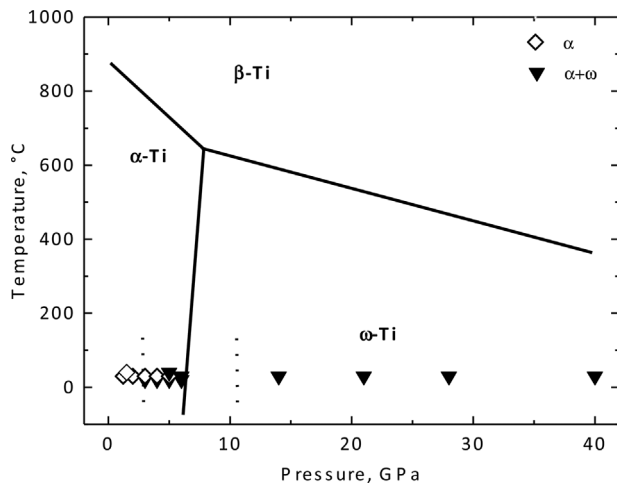


Fig. 1. Temperature–pressure equilibrium phase diagram for pure titanium. Thick solid lines mark the α - β , β - ω , and α - ω phase equilibrium based on the data obtained in situ under high pressure in hydrostatic conditions.^[4–13] Thin dotted lines reflect the scatter of experimental data for the pressure of α - ω transformation at room temperature. The experimental points mark the conditions of HPT treatment and demonstrate the phases present in the samples after HPT of pure or commercially pure titanium.^[17–23] These experimental points show the phases observed after finish of the anvils rotation and release of high-pressure. Diamonds are for the pure α -phase.^[17–19] Triangles are for the $\alpha + \omega$ mixture.^[17–23]

10.5 GPa, depending on the experimental technique, on the pressure environment, and on the sample purity (this interval is shown by vertical dotted lines at 2.9 and 10.5 GPa).^[8–13] The low temperature α -Ti crystallizes in the hexagonal closely packed (hcp) crystal structure (space group $P6_3/mmc$, Wyckoff positions 2c) with the ratio of the lattice parameters $c/a \approx 1.58$. Above 882 °C, the body-centered cubic (bcc) β -Ti is stable, which crystallizes in the space group $Im3m$, where the Ti atoms occupy the Wyckoff positions 2a. The crystal structure of ω -Ti is hexagonal (space group $P6/mmm$), and the Ti atoms occupy the Wyckoff positions 1a and 2d.^[8,14] The crystallographic mechanism of the $\alpha \leftrightarrow \omega$ (or $\alpha \leftrightarrow \beta \leftrightarrow \omega$) phase transformation was described in Refs.^[8,14] It was suggested that the $\alpha \rightarrow \omega$ transformation at low temperatures proceeds as $\alpha \rightarrow \beta \rightarrow \omega$. In other words, α -phase transforms into ω -phase through the formation of β -phase, which is thermodynamically unstable in pure titanium below 882 °C.^[8] The martensitic-type transformation is characterized by a rather large hysteresis; thus, the ω -phase can be retained in the material after release of the pressure.^[6] The experimental points in Figure 1 describe the results of the experiments of high-pressure torsion (HPT) of pure or commercially pure titanium and will be discussed below.

The Ti-Fe alloys are quite cheap among other Ti-based alloys doped with β -stabilizers. Most Ti-Fe binary alloys exhibit an excellent combination of high strength and large plasticity.^[15] Ti-Fe alloys are also useful for medical applications.^[16] Severe plastic deformation (SPD) by HPT permits to obtain the extremely fine-grained structure in Ti and Ti alloys.^[17–23] They also contain the high-pressure ω -

phase which remains quenched after release of high pressure. Moreover, SPD permits to drastically improve the mechanical properties of Ti and Ti-based alloys.^[24,25] In particular, the extraordinarily high strength and ductility has been achieved in nanograined Ti.^[24,25] The ω -phase appears after SPD also in Zr but not in Hf.^[26,27] If one would compare the phases in alloys before and after SPD with an equilibrium phase diagram, one could estimate the so-called effective temperature for the SPD treatment.^[28,29] The investigation of peculiarities of phase transformations in the SPD-treated Ti-Fe alloys was the goal of this work.

2. Experimental Section

Two Ti-Fe alloys with 1 and 10 wt% Fe were investigated. The alloys were inductively melted in vacuum of high purity components (99.9% Ti and 99.97% Fe). The melt was poured in vacuum into the water-cooled cylindrical copper crucible of 10 mm diameter. After sawing, grinding, and chemical etching, the 0.7 mm thick disks cut from the as-cast cylinders were deformed by HPT in a Bridgman anvil type unit (room temperature, pressure at 7 GPa, 5 torsions, 1 rotation-per-minute) using a custom built computer-controlled HPT device (W. Klement GmbH, Lang, Austria). Both alloys were also compressed in the same HPT machine without torsion at 7 GPa during 5 min. After HPT, the central (low-deformed) part of each disk (about 3 mm in diameter) was excluded from further investigations. The 2 mm thick slices were also cut from the \emptyset 10 mm cylindrical ingots and then divided into four parts. These as-cast samples were embedded in resin and then mechanically ground and polished, using 1 μ m diamond paste in the last polishing step, for the metallographic study. After etching, the as-cast samples were investigated by means of the scanning electron microscopy (SEM).

SEM investigations have been carried out in a Tescan Vega TS5130 MM microscope equipped with the LINK energy-dispersive X-ray spectrometer produced by Oxford Instruments. Samples for the transmission electron microscopy (TEM) were prepared by electropolishing in BK-2 non-acid electrolyte.^[30] TEM investigations were carried out using a TECNAI F2 electron microscope with acceleration voltage of 200 kV. X-ray diffraction patterns were obtained using Bragg-Brentano geometry in a powder diffractometer (Philips X'Pert) with Cu-K α radiation.

Both the as-cast samples and fine-grained HPT-treated samples were studied by differential thermal analysis (DTA) and differential scanning calorimetry (DSC) in the temperature range of 200–1100 °C using the DTA/TG SETSYS EVOLUTION 1750 (SETARAM, France) device and NETZSCH Pegasus 404C calorimeter. DTA measurements were performed in the dry argon or helium atmosphere, in Al₂O₃ crucibles and at the cooling and heating rates of 20 K min⁻¹. DSC was performed in Ar atmosphere and the same other conditions as for DTA. The results obtained by DTA and DSC were in perfect agreement with each other. DSC

investigations at 25–700 °C were performed in Netzsch 204 H calorimeter in He atmosphere with the heating rate of 10 K min⁻¹. The heating rate of 10 K min⁻¹ has been chosen because at the heating rates higher than 20 K min⁻¹, the temperatures of heat effects would be shifted toward higher temperature on heating and lower temperature on cooling. The lower heating rates of 5 or 1 K min⁻¹ led to the substantial grain growth in the HPT-treated samples. Additionally, the effects the authors would like to study became less visible at low heating/cooling rates.

3. Results

In Figure 2a and b, the SEM micrographs of the as-cast Ti–1 wt% Fe (Figure 2a) and Ti–10 wt% Fe (Figure 2b) alloys are

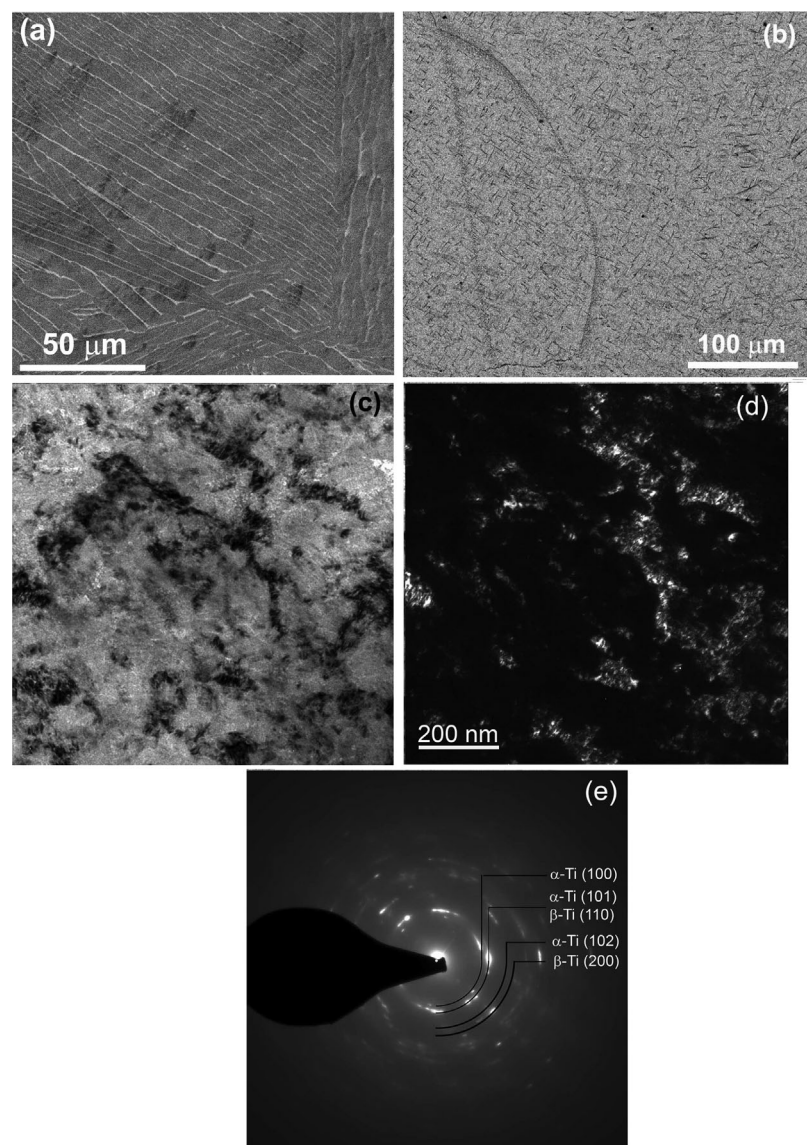


Fig. 2. SEM micrographs of the as-cast (a) Ti–1 wt% Fe and (b) Ti–10 wt% Fe alloys. The Ti-rich α -phase appears dark; the β -phase appears bright; (c) bright field, (d) dark field TEM micrographs, and (e) indexed electron diffraction pattern of the Ti–10 wt% Fe alloy after HPT.

shown. The Ti-rich α -phase appears dark and the β -phase appears bright. The as-cast Ti–1 wt% Fe alloy contains mainly the α -Ti-phase (Figure 2a). The structure consists of the lamella-shaped α -grains (about 100–200 μm long and 10 μm broad) separated by the thin β -lamellae with the thickness of 3–5 μm (Figure 2a). The alternating α - and β -lamellae form differently oriented colonies. The mean size of such an α/β -colony is about 300–500 μm . The as-cast Ti–10 wt% Fe alloy contains mainly the β -Ti-phase (Figure 2b). The size of β -Ti grains is about 100–300 μm . The α -phase forms the uniform layers with thickness of about 3–5 μm separating the β -grains (corresponding image is not shown here). This phenomenon is so-called complete wetting of β -Ti/ β -Ti grain boundaries by the second solid phase α -Ti.^[31–33] Additionally, the α -phase forms the numerous needle- or plate-like precipitates in the volume of β -grains. They have a length of \approx 10–30 μm and thickness of \approx 2–5 μm . The needles (plates) are parallel or perpendicular to each other; it is the indication of a certain orientation relationship between α - and β - phases.

HPT drastically refined the grains (see the TEM micrographs in Figure 2c and strong broadening of XRD lines, especially like α (1,0,–1,0) or β (200) in Figure 3). Figure 2 shows also the bright field (c), dark field (d) TEM micrographs, and (e) indexed electron diffraction pattern of the Ti–10 wt% Fe alloy after HPT. The dark field image was taken using the brightest reflections of both α - and β -phases. Unfortunately, it was not possible to separate the reflections from these two phases due to their vicinity (see Figure 2e). The size of slightly elongated α - and β -grains is about 100–150 nm. Therefore, both Ti–Fe alloys became ultra-fine grained. This grain size is close to the values previously obtained after HPT of commercially pure titanium (100–120 nm after HPT at 6 GPa, 5 turns, 1 rpm, 20–300 °C,^[18] 120 nm after HPT at 5 GPa, 5 turns, 1 rpm, 20 °C,^[19,20] 100–200 nm after HPT at 1, 5, and 5 GPa, 10 turns, 0.2 rpm, 20 °C,^[21,22] 50–150 nm after HPT at 3, 4, 5, and 6 GPa, 0.5–10 turns, 1 rpm, 20 °C^[23]), and of 99.4 wt% pure titanium (200 nm after HPT at 1.2 GPa and 150 nm after HPT at 6 GPa, 0.5–10 turns, 0.2 and 0.5 rpm, 20 °C^[17]).

XRD-patterns demonstrated that the coarse-grained (initial) as-cast alloy with 1% Fe contained mainly α -Ti with hcp lattice with a small amount of cubic β -Ti (Figure 3a). After uniaxial compression of this alloy (7 GPa without torsion), a redistribution of the integral intensities between the XRD peaks (110) and (200) of the β -phase took place in favor of the first one. This redistribution of the peaks

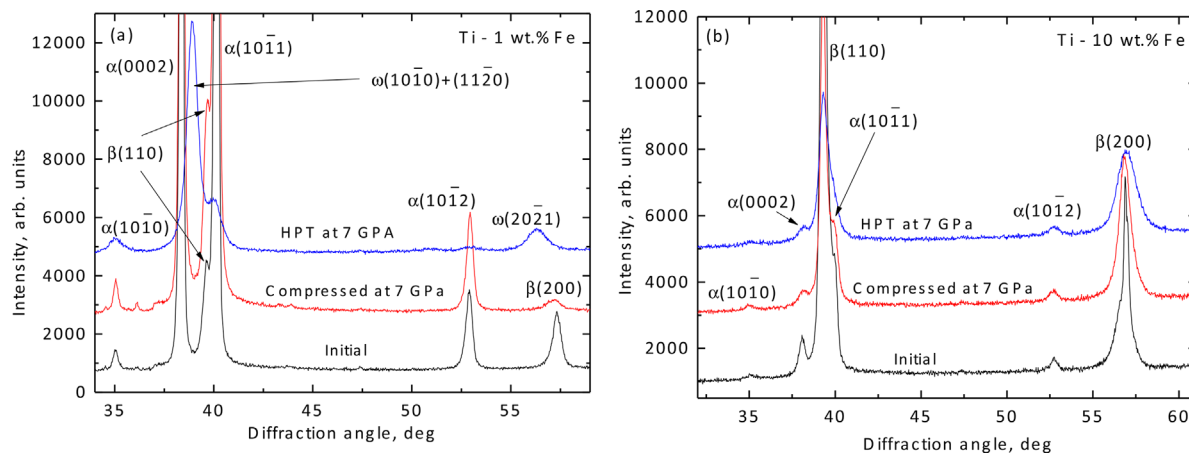


Fig. 3. X-ray diffraction patterns of (a) Ti-1 wt% Fe and (b) Ti-10 wt% Fe alloys in the as-cast (initial) state, after uniaxial compression at 7 GPa and after HPT. The patterns are vertically shifted for better comparison.

intensities could be the indication of weak $\langle 110 \rangle$ texture. It should be noted here that according to the theoretical predictions, the $\langle 110 \rangle$ texture component plays an important role for the $\alpha \rightarrow \beta \rightarrow \omega$ -phase transformation via the atomic shuffling within the $(0001)_\alpha$ planes.^[14] This is expected for the transformation pathways obeying one of the orientation relationships $(0001)_\alpha \parallel (110)_\beta \parallel (01\bar{1}1)_\omega$ or $(0001)_\alpha \parallel (011)_\beta \parallel (11\bar{2}0)_\omega$ pathways.^[14] After HPT, the majority of α -Ti transformed into ω -Ti, only minor amount of α -Ti remained, β -Ti completely disappeared.

The coarse-grained (initial) as-cast alloy with 10% Fe contained almost exclusively β -Ti with a small amount of α -Ti (Figure 3b). The weak peaks of α -Ti are shifted due to the alloying with Fe. After uniaxial compression of the Ti-10 wt% Fe alloy, the portion of α -Ti increased, that of β -Ti decreased. The ω -Ti was absent (see also TEM results in Figure 2c-e). The redistribution of intensity between peaks of β -phase (like that in the Ti-1 wt% Fe alloy) was not observed. After HPT, the Ti-10 wt% Fe alloy still contained only the α -Ti + β -Ti mixture, again without any sign of ω -Ti. Therefore, the alloying of Ti with big amounts of iron suppresses the formation of ω -Ti-phase during HPT.

In Figure 4, the results of thermal analysis are presented. The temperature dependencies of heat flow (heating curves) are shown for the initial as-cast, uniaxially compressed, and HPT-treated Ti-Fe alloys. It should be noted that no heat effect were observed on cooling for all investigated samples that is why cooling curves were not presented. Based on the results obtained during the second heating, it can be concluded that no reverse transformation occurred on cooling. All three high-temperature heating curves for the Ti-1 wt% Fe alloy are quite similar (Figure 4a) with some small decrease of the onset temperature in compressed and HPT-treated alloys. Each of them reveals one endothermic reaction (deep minimum), which starts around 841 °C (onset) and finishes close to 880 °C (peak). According to the equilibrium Ti-Fe phase diagram, this endothermic

transformation can be attributed as α -Ti to β -Ti transition.^[34] Indeed, according to the XRD data (Figure 3a), the initial Ti-1 wt% Fe alloy as well as the Ti-1 wt% Fe alloy after uniaxial compression contain only α -Ti. According to calculations based on thermodynamic data,^[34] the temperature of diffusionless transformation of α -Ti to β -Ti is equal to 793 °C. According to equilibrium calculations, transformation α -Ti + β -Ti \rightarrow β -Ti finishes at 860 °C. After HPT the Ti-1 wt% Fe alloy contains exclusively only ω -Ti (Figure 3a). The low-temperature heating curve for HPT-treated sample (Figure 4c) contains the exothermic peak around 143 °C. It has been shown earlier that in pure Ti, this exothermic reaction corresponds to the ω -Ti \rightarrow α -Ti transformation.^[23] By further temperature increase, the α -Ti transforms into β -Ti similar to the initial and compressed samples (Figure 4a). It should be noted that no transformation of β -Ti occurred during the second heating of Ti-1 wt% Fe samples.

In the Ti-10 wt% Fe alloy, the heating curves are more complicated (Figure 4b). All three samples reveal the combination of an exothermic reaction followed by the endothermic one. The exothermic reaction starts between ≈ 460 °C (HPT-treated sample) and 518 °C (initial sample). It should be noted that the exothermic effect is not very pronounced in case of the HPT-treated sample that makes it difficult to determine the onset. In the uniaxially compressed Ti-10 wt% Fe alloy, the exothermic reaction starts at 469 °C. XRD reveals that all Ti-10 wt% Fe samples contain large amounts of β -Ti (Figure 3b), which is absent in Ti-1 wt% Fe samples (Figure 3a). By heating, the metastable β -Ti first transforms into equilibrium α -Ti. Further heating leads to the equilibrium α -Ti \rightarrow α -Ti + β -Ti \rightarrow β -Ti transitions. Therefore, the exothermic maximum is immediately followed by the endothermic minimum in the curves shown in (Figure 4b). In accordance with the phase diagram, the α -Ti + β -Ti \rightarrow β -Ti transition occurs in the alloy Ti-1 wt% at higher temperature and in more narrow temperature range than in the Ti-10 wt% Fe alloy (see Figure 4a and b). The

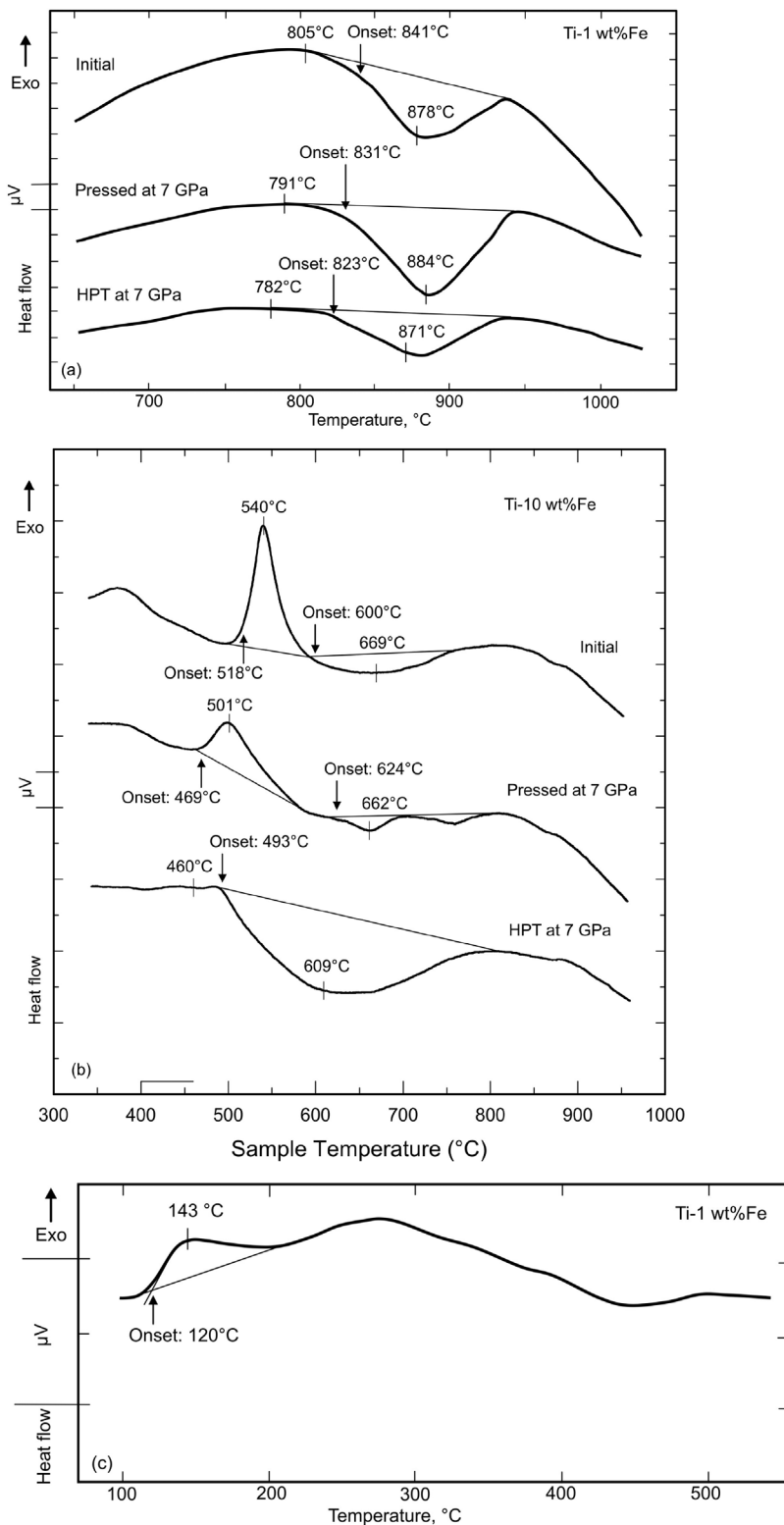


Fig. 4. The temperature dependencies of heat flow for (a) Ti-1 wt% Fe alloy, (b) Ti-10 wt% Fe alloy, and (c) Ti-1 wt% Fe alloy at low temperatures.

second heating of samples with 10 wt% Fe indicated more distinct exothermic effects attributed to transformation of β -Ti to α -Ti with some shift to higher temperature in comparison with first heating. It should be mentioned that

at low temperature, transformations in both alloys do not correspond to the phase diagram, and comparison with equilibrium diagram is only possible after metastable β -Ti transforms to equilibrium assemblage α -Ti + β -Ti.

4. Discussion

Figure 1 shows the results of the HPT treatment for pure titanium published in the literature.^[17-23] Full symbols mark the conditions of HPT treatment and demonstrate the phases present in the samples after HPT (i.e., observed after pressure release).^[17-23] Diamonds are for the pure α -phase.^[17-19] Triangles are for the $\alpha + \omega$ mixture.^[17-23] The HPT of commercially pure titanium at slow speed of 0.2 rpm and high strain of 10 turns resulted in α -phase at 1.5 GPa (diamond in Figure 1) and ω -phase with small amount of α -phase at 5 GPa (triangle in Figure 1).^[29,30] The HPT (0.5-10 turns, 0.2 and 0.5 rpm, 20 °C) of 99.4 wt% pure titanium in the range between 1.2 and 40 GPa permitted to observe the transition from pure α -Ti in the pressure range between 1.2 and 5 GPa (diamonds in Figure 1) to the two-phase α -Ti + ω -Ti mixture in the pressure range from 6 to 40 GPa (down triangles in Figure 1).^[17] Upon that the amount of α -Ti in samples deformed at 14, 21, 28, and 40 GPa was very low.^[17] The two-phase α -Ti + ω -Ti mixture (down triangles in Figure 1) has been observed after HPT of commercially pure titanium in Ref.^[23] The amount of ω -Ti grew from zero (diamond in Figure 1) at 3 GPa to 70% at 6 GPa by constant number of anvil turns of 5. The amount of ω -Ti also grew at 6 GPa from 55% after 0.5 anvil turn to 90% after 10 anvil turns. It has to be underlined that α -Ti still can be found in the samples together with ω -Ti even after HPT at 40 GPa.^[17] Most probably, it appears due to the reversal ω -Ti \rightarrow α -Ti transformation after pressure release at the end of HPT treatment.

It is well known that the $\alpha \rightarrow \omega$ phase transformation is of martensitic (diffusionless) type, and the ω -Ti is in equilibrium at room temperature above 7.4 ± 2 GPa (Figure 1).^[4-13] Obviously, the reason for the formation of the ω -phase during HPT at significantly lower pressures is related to a considerable contribution in the thermodynamic driving force provided by the external shear stress.^[23] It is known that shear stress can facilitate the martensitic transformations,^[35] and

enhancement of the $\alpha \rightarrow \omega$ transition in the presence of external shear stress has been shown previously.^[12,17-23] It has been also predicted theoretically^[36] basing on the ab initio calculations employing the density functional theory (DFT) that the alloying with β -stabilizer elements such as V, Mo, Fe, and Ta should lead to a decrease in the onset pressure of the $\alpha \rightarrow \omega$ transformation. However, it is not clear yet, why ω -Ti was not formed in the same HPT conditions in Ti-10 wt% Fe alloy. It happens despite of the fact that Ti-10 wt% Fe alloy contained mostly β -Ti. The mechanism of $\beta \rightarrow \omega$ transformation at present is not known. Some authors discussed the possibility of the β -Ti formation as the intermediate product of the $\alpha \rightarrow \omega$ transformation taking place at temperatures below 882 °C, where this phase is thermodynamically unstable.^[8] Our study had shown that this scenario is rather implausible, as soon as we observed $\alpha \rightarrow \omega$ transformation, and not the $\beta \rightarrow \omega$ at identical conditions of HPT.

5. Conclusions

- 1) SPD by HPT leads to the strong grain refinement in Ti-Fe alloys.
- 2) The high-pressure ω -Ti-phase appears during HPT and remains quenched in the Ti-1 wt% Fe alloy at the ambient pressure.
- 3) The high-pressure ω -Ti-phase disappears by heating around 143 °C.
- 4) The Ti-10 wt% Fe alloy contains the α -Ti + β -Ti mixture in the initial state, after compression and after HPT; however, the ω -Ti does not appear even after HPT. It means that the addition of Fe suppresses the formation of ω -Ti during HPT.

Article first published online: June 23, 2015

Manuscript Revised: April 19, 2015

Manuscript Received: March 18, 2015

- [1] N. M. Beskorovainyi, B. A. Kalin, P. A. Platonov, I. I. Chernov, *Structural materials for nuclear reactors*, Energoatomizdat, Moscow **1995** (in Russian).
- [2] R. Boyer, E. W. Collings, G. Welsch, *Materials Properties Handbook: Titanium Alloys*, ASM International, Materials Park, Ohio **1994**.
- [3] M. J. Donachie, *Titanium: A Technical Guide*, 2nd ed., ASM International, Materials Park, Ohio **2000**.
- [4] A. R. Kutsar, M. N. Pavlovskii, V. V. Komissarov, *JETP Lett.* **1982**, 35, 108.
- [5] S. K. Sikka, Y. K. Vohra, R. Chidambaram, *Prog. Mater. Sci.* **1982**, 27, 245.
- [6] J. C. Jamieson, *Science* **1963**, 140, 72.
- [7] A. Jayaraman, W. Clement, G. C. Kennedy, *Phys. Rev.* **1963**, 131, 644.
- [8] M. P. Usikov, V. A. Zilbershtein, *Phys. Status Sol. A* **1973**, 19, 53.
- [9] H. Xia, G. Parthasarathy, H. Luo, Y. K. Vohra, A. L. Ruoff, *Phys. Rev. B* **1990**, 42, 6736.
- [10] J. Zhang, Y. Zhao, R. S. Hixson, G. T. Gray III, L. Wang, U. Wataru, H. Saito, T. Hattori, *J. Phys. Chem. Sol.* **2008**, 69, 2559.
- [11] Y. K. Vohra, S. K. Sikka, S. N. Vaidya, R. Chidambaram, *J. Phys. Chem. Sol.* **1977**, 38, 1293.
- [12] D. Errandonea, Y. Meng, M. Somayazulu, D. Häusermann, *Physica B* **2005**, 355, 116.
- [13] N. Velisavljevic, S. MacLeod, H. Cynn, in: *Titanium Alloys—Towards Achieving Enhanced Properties for Diversified Applications*, (Ed: N. Amin), InTech, Rijeka, Croatia **2012**, pp. 67–86.
- [14] D. R. Trinkle, R. G. Hennig, S. G. Srinivasan, D. M. Hatch, M. D. Jones, H. T. Stokes, R. C. Albers, J. W. Wilkins, *Phys. Rev. Lett.* **2003**, 91, 025701.
- [15] L.-C. Zhang, *Adv. Mater. Res.* **2012**, 1, 13.
- [16] M. Koike, Ch. Ohkubo, H. Sato, H. Fujii, T. Okabe, *Mater. Sci. Eng. C* **2005**, 25, 349.
- [17] K. Edalati, E. Matsubara, Z. Horita, *Metal. Mater. Trans. A* **2009**, 40, 2079.
- [18] R. K. Islamgaliev, V. U. Kazyhanov, L. O. Shestakova, A. V. Sharafutdinov, R. Z. Valiev, *Mater. Sci. Eng. A* **2008**, 493, 190.
- [19] A. V. Sergueeva, V. V. Stolyarov, R. Z. Valiev, A. K. Mukherjee, *Scr. Mater.* **2001**, 45, 747.
- [20] R. Z. Valiev, A. V. Sergueeva, A. K. Mukherjee, *Scr. Mater.* **2003**, 49, 669.
- [21] I. Todaka, J. Sasaki, T. Moto, M. Umemoto, *Scr. Mater.* **2008**, 59, 615.
- [22] I. Todaka, M. Umemoto, A. Yamazaki, J. Sasaki, K. Tsuchiya, *Mater. Trans.* **2008**, 49, 47.
- [23] Y. Ivanisenko, A. Kilmametov, H. Roesner, R. Z. Valiev, *Int. J. Mater. Res.* **2008**, 99, 36.
- [24] R. Z. Valiev, *Nat. Mater. Res.* **2004**, 3, 511.
- [25] R. Z. Valiev, I. V. Alexandrov, Y. T. Zhu, T. C. Lowe, *J. Mater. Res.* **2002**, 17, 5.
- [26] K. Edalati, Z. Horita, Y. Mine, *Mater. Sci. Eng. A* **2010**, 527, 2136.
- [27] A. P. Zhilyaev, I. Sabirov, G. González-Doncela, J. Molina-Aldareguía, B. Srinivasarao, M. T. Pérez-Prado, *Mater. Sci. Eng. A* **2011**, 528, 3496.
- [28] B. B. Straumal, A. A. Mazilkin, B. Baretzky, E. Rabkin, R. Z. Valiev, *Mater. Trans.* **2012**, 53, 63.
- [29] B. Straumal, A. Korneva, P. Zięba, *Arch. Civil Mech. Eng.* **2014**, 14, 242.
- [30] B. J. Kestel, *Ultramicroscopy* **1986**, 19, 205.
- [31] B. B. Straumal, A. S. Gornakova, Y. O. Kucheev, B. Baretzky, A. N. Nekrasov, *J. Mater. Eng. Perform.* **2012**, 21, 721.
- [32] B. B. Straumal, B. Baretzky, O. A. Kogtenkova, A. B. Straumal, A. S. Sidorenko, *J. Mater. Sci.* **2010**, 45, 2057.

- [33] G. A. López, E. J. Mittemeijer, B. B. Straumal, *Acta Mater.* **2004**, *52*, 4537.
- [34] Scientific Group Thermodata Europe, Landolt-Börnstein Group IV, *Physical Chemistry Vol. 19 Thermodynamic Properties of Inorganic Materials, Subvolume B, Binary systems, Part 3, Binary systems from Cs-K to Mg-Zr*, Springer, Berlin/Heidelberg **2005**.
- [35] J. R. Patel, M. Cohen, *Acta Metal.* **1953**, *1*, 531.
- [36] R. Hennig, D. R. Trinkle, J. Bouchet, S. G. Srinivasan, R. C. Albers, J. W. Wilkins, *Nat. Mater.* **2005**, *4*, 129.
-